

Analytical Modeling of I - V characteristics using 2D Poisson Equations in AlN/ β -Ga₂O₃ HEMT

¹R. Singh, ¹T. R. Lenka, ²D. K. Panda, ³H. P. T. Nguyen, ⁴N. El. I. Boukourt, ⁵G. Crupi

¹Department of Electronics and Communication Engineering, National Institute of Technology
Silchar Assam, India (Email: rajan_rs@ece.nits.ac.in , trlenka@ieee.org)

²School of Electronics, VIT-AP University, Amaravati, AP, 522237 India (deepak.panda@vitap.ac.in)

³Department of Electrical and Computer Engineering, New Jersey Institute of Technology, Newark,
NJ 07102, USA (E-mail: hieu.p.nguyen@njit.edu)

⁴Electronics and Communication Engineering Department, Kuwait College of Science and
Technology, Doha, Kuwait (n.boukourt@kcst.edu.kw)

⁵BIOMORF Department, University of Messina, Messina 98125, Italy (E-mail: crupig@unime.it)

Abstract: In this paper, physics-based analytical models using two-dimensional (2D) Poisson equations for surface potential, channel potential, electric field, and drain current in AlN/ β -Ga₂O₃ high electron mobility transistor (HEMT) are presented. The analytical expression of different quantities is achieved based on full depletion approximation of the AlN barrier layer and polarization charge induced unified two-dimensional electron gas (2DEG) charge density model. For the validation of the developed model, results are compared with 2D numerical simulation results and a good consistency is found between the two. The drain current model is also validated with experimental results of a similar dimension device. The developed model can be a good reference for different β -Ga₂O₃-based HEMTs.

Keywords: 2DEG, AlN/ β -Ga₂O₃, HEMT, Poisson equation, Surface potential

1. Introduction

Nowadays, Gallium-oxide (Ga₂O₃) is being explored for its possible application in the decade-old high electron mobility transistors (HEMTs) technology, currently dominated by III-nitride material like gallium-nitride (GaN). GaN HEMTs have shown excellent performance for high power and high-frequency applications on the back of exciting features such as higher two-dimensional electron gas (2DEG) density $n_s \sim 10^{13} \text{ cm}^{-2}$, very high 2DEG mobility $\sim 1500 \text{ cm}^2/\text{Vs}$. However, rising emerging applications like electric vehicles (EVs) and robotics have expanded the investigation horizon from wide bandgap (WBG) to ultra-wide bandgap (UWB) semiconductors. Among the UWB semiconductors, β -Ga₂O₃ is found to be more suitable for high voltage applications due to its ultra-large bandgap of $\sim 4.9 \text{ eV}$, and breakdown field of $\sim 8 \text{ MV}$. Moreover, β -Ga₂O₃ single crystal substrate can be grown using melt-based techniques, which ensures large size and affordable wafers for different device technologies.

To date, various β -Ga₂O₃ based experimental devices like Schottky diodes [1], [2], metal-oxide-semiconductor field-effect transistors MOSFETs[3]–[6], and β -(Al_xGa_{1-x})₂O₃/Ga₂O₃ (AGO/GO) HEMTs [7], [8] with excellent DC and RF performances have been reported. However, since β -Ga₂O₃ does not have any polarization property, and small band offset in AGO/GO HEMTs limit their performance as compared to their AlGaN/GaN counterpart. On the other hand, epitaxial layers of III-nitrides (AlN, GaN, InN) have been grown on β -Ga₂O₃ and potential AlN/ β -Ga₂O₃ HEMT applications are anticipated [9]–[12]. Moreover, one of our

previous works in AlN/ β -Ga₂O₃ HEMT estimated exceptional RF performance—cut-off frequency f_T of 167 GHz, and output power P_{OUT} of 2.91 W/mm [13]. Since the 2DEG density n_s in HEMTs has a critical role in device operation, recently we have reported validation of estimated n_s in AlN/ β -Ga₂O₃ HEMT through analytical modeling in [14]. Various physics-based models for different parameters in AlGaIn/GaN HEMTs have been reported [15]–[20], but almost none for β -Ga₂O₃-based HEMTs. Looking at the accuracy of the mathematical models over empirical and approximation models, device physics-based mathematical models for β -Ga₂O₃ based HEMT will be useful to analyze and validate the estimated results. Here, we present physics-based mathematical models for surface potential and electric fields and extended them to get the current-voltage model in AlN/ β -Ga₂O₃ HEMT with an etched AlN barrier layer. For the validation of results, developed model results are compared with simulation as well as experimental results earlier published for similar β -Ga₂O₃ devices.

2. Device Structure

The cross-sectional schematic of the analysed device is shown in Fig. 1. The epi-layer sequence is as follows: on a semi-insulating β -Ga₂O₃ substrate an n-type doped 100 nm β -Ga₂O₃ buffer layer with $N_D = 1.5 \times 10^{16} / \text{cm}^3$ exists, followed by 10 nm AlN barrier layer which is undoped. Source and drain contacts are set as Ohmic with contact resistance of 0.4 Ω -mm. The gate contact is assumed as Schottky and a barrier potential of 0.8 eV is set. The device dimensions are kept the same as [5] with gate length L_G of 2.8 μm , gate-drain spacing L_{GD} of 1.3 μm , and gate-source spacing L_{GS} of 0.4 μm . The gate width W is equal to 100 μm , and the output drain current is normalized with this quantity. In the simulation framework different physics-based models like Shockley-Read-Hall (SRH) recombination, Fermi-Dirac for carrier statistics, and negative differential conductivity (NDC) to capture electron velocity saturation effect are evoked. Default material parameters and spontaneous as well as piezoelectric polarization models are used from [21] for AlN barrier material. The β -Ga₂O₃ material parameters used in the simulations and model development are taken from [22], [23], Table 1.

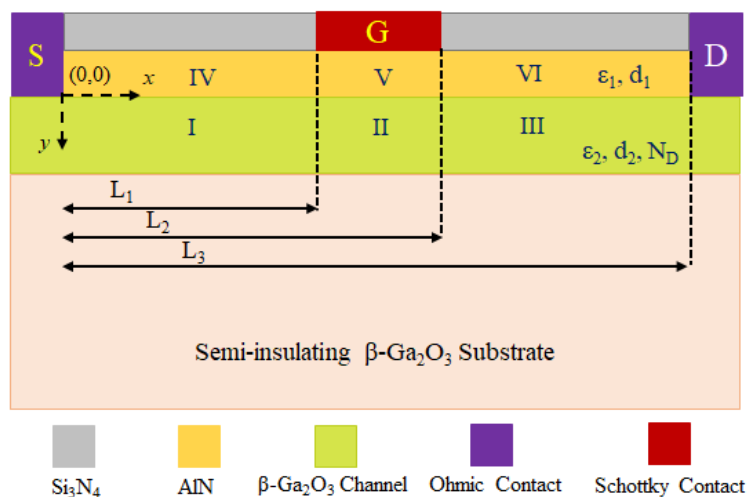


Fig. 1: 2D cross-sectional view of AlN/ β -Ga₂O₃ HEMT.

Table 1. Material parameters for β -Ga₂O₃ [22], [23].

Symbol	Quantity	Values	Symbol	Quantity	Values
E_g	Energy bandgap	4.9 eV	N_V	Valence band density	2.86×10^{18}

χ	Electron affinity	3.15 eV	ϵ_r	Relative permittivity	10
m_e^*	Electron effective mass	$0.25m_0$	a_0	Lattice constant	3.04
D	Density of states	$1.045 \times 10^{18} \text{ m}^{-2} \text{ V}^{-1}$	μ_{n0}	Electron mobility	$140 \text{ cm}^2 / \text{Vs}$
N_C	Conduction band density	3.13×10^{18}	μ_{p0}	Hole mobility	$50 \text{ cm}^2 / \text{Vs}$

A list of symbols used in the model development is given in Table 2.

Table 2. Symbols used in analytical modeling

Symbol	Quantity	Symbol	Quantity
ϵ_1, ϵ_2	Permittivity of AlN and $\beta\text{-Ga}_2\text{O}_3$ material respectively	q	Unit electron charge
d_1, d_2	Thickness of AlN and $\beta\text{-Ga}_2\text{O}_3$ layer respectively	V_{FB}	Flat band voltage
N_D	Channel doping concentration	V_{bi}	Built-in potential
Φ_m	Gate metal workfunction	E_F	Fermi potential
n_s	2DEG density	k	Boltzmann constant
V_{OFF}	Threshold voltage	ΔE_C	Conduction band offset
V_{th}	Thermal voltage	χ	Electron affinity
C_G	Gate capacitance	T	Temperature

A physics-based analytical model for surface potential, electric field, and drain current are developed by solving two-dimensional (2-D) Poisson's equation in the channel region marked as Region I, II, and III as shown in Fig. 1. The 2-D Poisson's equation for the potential function $\varphi(x, y)$ in the channel ($0 \leq x \leq L_3$) is given by:

$$\frac{d^2\varphi_i(x, y)}{dx^2} + \frac{d^2\varphi_i(x, y)}{dy^2} = -\frac{qN_D}{\epsilon_2}, \quad i = 1, 2, 3 \quad (1)$$

$$\frac{d^2\varphi_i(x, y)}{dx^2} + \frac{d^2\varphi_i(x, y)}{dy^2} = 0, \quad i = 4, 5, 6 \quad (2)$$

where N_D , and ϵ_2 are doping concentration and permittivity of $\beta\text{-Ga}_2\text{O}_3$ buffer layer. Since potential at the AlN/ $\beta\text{-Ga}_2\text{O}_3$ interface is continuous, it is only solved for the region I, II, and III.

The potential function $\varphi(x, y)$ along the y-direction in the channel can be approximated by a parabolic expression such as:

$$\varphi_i(x, y) = \varphi_{si}(x) + A_i(x)y + A_{i+1}(x)y^2, \text{ for } i = 1, 2, 3 \quad (3)$$

where $\varphi_{si}(x)$ are the surface potential, and $A_i(x)$ are arbitrary constants for the region I, II, and III that are to be determined using boundary conditions. The Poisson's equation (1) is solved simultaneously for all three regions in the channel using solution expressed in (3), and given as:

$$\varphi_1(x, y) = \varphi_{s1}(x) + A_1(x)y + A_2(x)y^2, \text{ for } 0 \leq x \leq L_1 \quad (4)$$

$$\varphi_2(x, y) = \varphi_{s2}(x) + A_3(x)y + A_4(x)y^2, \text{ for } L_1 \leq x \leq L_2 \quad (5)$$

$$\varphi_3(x, y) = \varphi_{s3}(x) + A_5(x)y + A_6(x)y^2, \text{ for } L_2 \leq x \leq L_3 \quad (6)$$

where $\varphi_1(x, y)$, $\varphi_2(x, y)$, $\varphi_3(x, y)$ and $\varphi_{s1}(x)$, $\varphi_{s2}(x)$, $\varphi_{s3}(x)$ are the channel potential and surface potential in the channel in the region I, II, and III respectively. Furthermore, above equations (4), (5), and (6) are solved using the following boundary conditions for $\varphi_i(x, y)$ are given by:

$$\left. \frac{d\varphi_1(x, y)}{dy} \right|_{y=0} = \frac{\varepsilon_1}{\varepsilon_2} \frac{\varphi_{s1}(x) - V'_{GS}}{d_1} \quad (7)$$

$$\left. \frac{d\varphi_1(x, y)}{dy} \right|_{y=-d_1} = \frac{-qn_{s1}}{\varepsilon_1} = -E_1 \quad (8)$$

$$\left. \frac{d\varphi_2(x, y)}{dy} \right|_{y=0} = \frac{\varepsilon_1}{\varepsilon_2} \frac{\varphi_{s2}(x) - V'_{GS}}{d_1} \quad (9)$$

$$\left. \frac{d\varphi_2(x, y)}{dy} \right|_{y=-d_1} = \frac{-qn_{s2}}{\varepsilon_1} = -E_2 \quad (10)$$

$$\left. \frac{d\varphi_3(x, y)}{dy} \right|_{y=0} = \frac{\varepsilon_1}{\varepsilon_2} \frac{\varphi_{s3}(x) - V'_{GS}}{d_1} \quad (11)$$

$$\left. \frac{d\varphi_3(x, y)}{dy} \right|_{y=-d_1} = \frac{-qn_{s1}}{\varepsilon_1} = -E_3 \quad (12)$$

$$\varphi_{s1}(x)|_{x=0} = V_{bi} \quad (13)$$

$$\varphi_{s1}(x)|_{x=L_3} = V_{DS} + V_{bi} \quad (14)$$

$$V'_{GS} = V_{GS} - V_{FB} \quad (15)$$

where $V_{FB} = \Phi_m - \Phi_{s1}$, where $\Phi_{s1} = \chi_1 + E_{G1}/2$, since the AlN barrier layer is undoped.

Since $\beta\text{-Ga}_2\text{O}_3$ does not possess any polarization property, the total polarization charge of the AlN/ $\beta\text{-Ga}_2\text{O}_3$ heterostructure is a sum of spontaneous as well as piezoelectric polarization of the AlN barrier layer. Total polarization of the AlN barrier $P_T = P_{sp} + P_{pi}$, where spontaneous polarization $P_{sp} = -0.09 \text{ C/m}^2$ [21], and piezoelectric polarization P_{pi} is calculated as given in [21]:

$$P_{pi} = 2 \left(\frac{a_s - a_0}{a_0} \right) e_{31} - \frac{C_{13}}{C_{33}} e_{33} \quad (16)$$

where a_s , a_0 are lattice constants of AlN and $\beta\text{-Ga}_2\text{O}_3$; e_{31} , e_{33} and C_{13} , C_{33} are piezoelectric and elastic constants for AlN material respectively.

Based on full depletion of the AlN barrier layer, the polarization induced 2DEG charge density is given by [17]

$$n_s = \frac{\varepsilon_1}{qd_1} (V_{GO} - E_F - \varphi_i(x)) \quad (17)$$

where $V_{GO} = V_{GS} - V_{OFF}$, and $\varphi_i(x)$ is the channel potential in regions I, II, III for $i = 1, 2, 3$. Furthermore, cut-off voltage V_{OFF} is given as

$$V_{OFF} = \Phi_B - \Delta E_C - \frac{P_T}{C_G} \quad (18)$$

Where Φ_B is the Schottky barrier height; ΔE_C is the conduction band offset between AlN and β -Ga₂O₃ at the heterointerface; P_T is the total polarization charge density, and C_G is the gate capacitance.

Since surface potential and the lateral electric field between the two consecutive regions at the heterointerface are continuous. The associated boundary conditions at the interface of region I-II and region II-III are given as

$$\varphi_{s1}(x)|_{x=L_1} = \varphi_{s2}(x)|_{x=L_2} \quad (19)$$

$$\left. \frac{d\varphi_{s1}(x)}{dx} \right|_{x=L_1} = \left. \frac{d\varphi_{s2}(x)}{dx} \right|_{x=L_1} \quad (20)$$

$$\varphi_{s2}(x)|_{x=L_2} = \varphi_{s3}(x)|_{x=L_2} \quad (21)$$

$$\left. \frac{d\varphi_{s2}(x)}{dx} \right|_{x=L_2} = \left. \frac{d\varphi_{s3}(x)}{dx} \right|_{x=L_2} \quad (22)$$

Now using boundary conditions of (7) to (12), all six constants of (4) to (6) are determined to get the AlN/ β -Ga₂O₃ HEMT channel potential as

$$\varphi_1(x, y) = \varphi_{s1}(x) + \frac{\varepsilon_1}{\varepsilon_2} \left(\frac{\varphi_{s1}(x) - V'_{GS}}{2d_1} \right) y + \left\{ \frac{-E_1}{2d_1} + \frac{\varepsilon_1}{\varepsilon_2} \left(\frac{\varphi_{s1}(x) - V'_{GS}}{2d_1} \right) \right\} y^2 \quad (23)$$

$$\varphi_2(x, y) = \varphi_{s2}(x) + \frac{\varepsilon_1}{\varepsilon_2} \left(\frac{\varphi_{s2}(x) - V'_{GS}}{2d_1} \right) y + \left\{ \frac{-E_2}{2d_1} + \frac{\varepsilon_1}{\varepsilon_2} \left(\frac{\varphi_{s1}(x) - V'_{GS}}{2d_1} \right) \right\} y^2 \quad (24)$$

$$\varphi_3(x, y) = \varphi_{s3}(x) + \frac{\varepsilon_1}{\varepsilon_2} \left(\frac{\varphi_{s3}(x) - V'_{GS}}{2d_1} \right) y + \left\{ \frac{-E_3}{2d_1} + \frac{\varepsilon_1}{\varepsilon_2} \left(\frac{\varphi_{s1}(x) - V'_{GS}}{2d_1} \right) \right\} y^2 \quad (25)$$

Now substituting values of the channel potential obtained above in (1), new equations for the region I, II, and III are obtained as

For region I ($0 \leq x \leq L_1$)

$$\frac{d^2\varphi_{s1}(x)}{dx^2} - \frac{\varepsilon_1}{\varepsilon_2 d_1^2} \varphi_{s1}(x) = \frac{\varepsilon_1}{\varepsilon_2 d_1^2} \left\{ \frac{-qN_D}{\varepsilon_2} \frac{\varepsilon_2 d_1^2}{\varepsilon_1} + \frac{E_1}{d_1} \frac{\varepsilon_2 d_1^2}{\varepsilon_1} - V'_{GS} \right\} \quad (26)$$

For region II ($L_1 \leq x \leq L_2$)

$$\frac{d^2\varphi_{s2}(x)}{dx^2} - \frac{\varepsilon_1}{\varepsilon_2 d_1^2} \varphi_{s2}(x) = \frac{\varepsilon_1}{\varepsilon_2 d_1^2} \left\{ \frac{-qN_D}{\varepsilon_2} \frac{\varepsilon_2 d_1^2}{\varepsilon_1} + \frac{E_2}{d_1} \frac{\varepsilon_2 d_1^2}{\varepsilon_1} - V'_{GS} \right\} \quad (27)$$

For region III ($L_2 \leq x \leq L_3$)

$$\frac{d^2\varphi_{s3}(x)}{dx^2} - \frac{\varepsilon_1}{\varepsilon_2 d_1^2} \varphi_{s3}(x) = \frac{\varepsilon_1}{\varepsilon_2 d_1^2} \left\{ \frac{-qN_D}{\varepsilon_2} \frac{\varepsilon_2 d_1^2}{\varepsilon_1} + \frac{E_3}{d_1} \frac{\varepsilon_2 d_1^2}{\varepsilon_1} - V'_{GS} \right\} \quad (28)$$

The solutions of equations (26) – (28) are obtained using the sum of complementary function (CF) and particular integral (PI) and given as follows

$$\varphi_{s1}(x) = Ae^{k_1x} + Be^{-k_1x} - p_1 \quad (29)$$

$$\varphi_{s2}(x) = Ce^{k_2x} + De^{-k_2x} - p_2 \quad (30)$$

$$\varphi_{s3}(x) = Ee^{k_3x} + Fe^{-k_3x} - p_3 \quad (31)$$

Where

$$k_1^2 = k_2^2 = \frac{\varepsilon_1}{\varepsilon_2 d_1^2} \quad (32)$$

$$p_1 = p_3 = \frac{-qN_D}{\varepsilon_2 k_1^2} + \frac{E_1}{d_1 k_1^2} - V'_{GS} \quad (33)$$

$$p_2 = \frac{-qN_D}{\varepsilon_2 k_2^2} + \frac{E_2}{d_1 k_2^2} - V'_{GS} \quad (34)$$

Now the constants of (29) – (31) are calculated using boundary conditions given in (13), (14) and (19) – (22), and given as

$$A = \frac{e^{-k_1 L_3}}{e^{-k_1 L_3} - e^{k_1 L_3}} \left(V_{bi} + p_1 + \frac{p_2 - p_1}{2e^{-k_1 L_1}} + \frac{p_3 - p_2}{2e^{-k_1 L_2}} \right) - \frac{e^{k_1 L_3}}{e^{-k_1 L_3} - e^{k_1 L_3}} \left(\frac{p_1 - p_2}{2e^{k_1 L_1}} + \frac{p_2 - p_3}{2e^{k_1 L_2}} \right) - \left(\frac{V_{bi} + V_{DS} + p_3}{e^{-k_1 L_3} - e^{k_1 L_3}} \right) \quad (35)$$

$$B = \frac{e^{k_1 L_3}}{e^{k_1 L_3} - e^{-k_1 L_3}} (V_{bi} + p_1) - \frac{e^{-k_1 L_3}}{e^{-k_1 L_3} - e^{k_1 L_3}} \left(\frac{p_2 - p_1}{2e^{-k_1 L_1}} + \frac{p_3 - p_2}{2e^{-k_1 L_2}} \right) - \frac{e^{k_1 L_3}}{e^{-k_1 L_3} - e^{k_1 L_3}} \left(\frac{p_1 - p_2}{2e^{k_1 L_1}} + \frac{p_2 - p_3}{2e^{k_1 L_2}} \right) - \left(\frac{V_{bi} + V_{DS} + p_3}{e^{-k_1 L_3} - e^{k_1 L_3}} \right) \quad (36)$$

$$C = \frac{e^{-k_1 L_3}}{e^{-k_1 L_3} - e^{k_1 L_3}} \left(V_{bi} + p_1 + \frac{p_2 - p_1}{2e^{-k_1 L_1}} + \frac{p_3 - p_2}{2e^{-k_1 L_2}} \right) - \frac{e^{-k_1 L_3}}{e^{-k_1 L_3} - e^{k_1 L_3}} \left(\frac{p_1 - p_2}{2e^{k_1 L_1}} \right) - \frac{e^{k_1 L_3}}{e^{-k_1 L_3} - e^{k_1 L_3}} \left(\frac{p_2 - p_3}{2e^{k_1 L_2}} \right) - \left(\frac{V_{bi} + V_{DS} + p_3}{e^{-k_1 L_3} - e^{k_1 L_3}} \right) \quad (37)$$

$$D = \frac{e^{k_1 L_3}}{e^{k_1 L_3} - e^{-k_1 L_3}} (V_{bi} + p_1) - \frac{e^{k_1 L_3}}{e^{-k_1 L_3} - e^{k_1 L_3}} \left(\frac{p_2 - p_1}{2e^{-k_1 L_1}} \right) - \frac{e^{-k_1 L_3}}{e^{-k_1 L_3} - e^{k_1 L_3}} \left(\frac{p_3 - p_2}{2e^{-k_1 L_2}} \right) - \frac{e^{k_1 L_3}}{e^{-k_1 L_3} - e^{k_1 L_3}} \left(\frac{p_1 - p_2}{2e^{k_1 L_1}} + \frac{p_2 - p_3}{2e^{k_1 L_2}} \right) - \left(\frac{V_{bi} + V_{DS} + p_3}{e^{-k_1 L_3} - e^{k_1 L_3}} \right) \quad (38)$$

$$E = \frac{e^{-k_1 L_3}}{e^{-k_1 L_3} - e^{k_1 L_3}} \left(V_{bi} + p_1 + \frac{p_2 - p_1}{2e^{-k_1 L_1}} + \frac{p_3 - p_2}{2e^{-k_1 L_2}} \right) - \frac{e^{-k_1 L_3}}{e^{-k_1 L_3} - e^{k_1 L_3}} \left(\frac{p_1 - p_2}{2e^{k_1 L_1}} \right) - \frac{e^{k_1 L_3}}{e^{-k_1 L_3} - e^{k_1 L_3}} \left(\frac{p_2 - p_3}{2e^{k_1 L_2}} \right) - \left(\frac{V_{bi} + V_{DS} + p_3}{e^{-k_1 L_3} - e^{k_1 L_3}} \right) \quad (39)$$

$$F = \frac{e^{k_1 L_3}}{e^{k_1 L_3} - e^{-k_1 L_3}} (V_{bi} + p_1) - \frac{e^{k_1 L_3}}{e^{-k_1 L_3} - e^{k_1 L_3}} \left(\frac{p_2 - p_1}{2e^{-k_1 L_1}} \right) - \frac{e^{k_1 L_3}}{e^{-k_1 L_3} - e^{k_1 L_3}} \left(\frac{p_3 - p_2}{2e^{-k_1 L_2}} \right) - \frac{e^{k_1 L_3}}{e^{-k_1 L_3} - e^{k_1 L_3}} \left(\frac{p_1 - p_2}{2e^{k_1 L_1}} + \frac{p_2 - p_3}{2e^{k_1 L_2}} \right) - \left(\frac{V_{bi} + V_{DS} + p_3}{e^{-k_1 L_3} - e^{k_1 L_3}} \right) \quad (40)$$

3. Analysis of Surface Potential, Channel Potential, Electric Field, and Drain Current

Now the surface potential for the entire channel length ($x = 0$ to L_3) using (29), (30), (31) is given as

$$\varphi_s(x) = \varphi_{s1}(x) + \varphi_{s2}(x) + \varphi_{s3}(x) \quad (41)$$

Furthermore, using (23), (24), and (25) and substituting $y = d_1$, the channel potential for entire channel length ($x = 0$ to L_3) is given as

$$\varphi(x, d_1) = \varphi_1(x, d_1) + \varphi_2(x, d_1) + \varphi_3(x, d_1) \quad (42)$$

where channel potential for the region I, II, and III are given as

$$\varphi_1(x, d_1) = \varphi_{s1}(x) + \frac{\varepsilon_1}{\varepsilon_2} (\varphi_{s1}(x) - V'_{GS}) + \frac{-E_1}{2} \quad (43)$$

$$\varphi_2(x, d_1) = \varphi_{s2}(x) + \frac{\varepsilon_1}{\varepsilon_2} (\varphi_{s2}(x) - V'_{GS}) + \frac{-E_2}{2} \quad (44)$$

$$\varphi_3(x, d_1) = \varphi_{s3}(x) + \frac{\varepsilon_1}{\varepsilon_2} (\varphi_{s3}(x) - V'_{GS}) + \frac{-E_3}{2} \quad (45)$$

The lateral electric field along the 2DEG channel can be defined as

$$E_x = -\frac{d\varphi(x)}{dx} \quad (46)$$

And from $x = 0$ to L_3 , the x component of the electric field is given as

$$E_x = E_{x1} + E_{x2} + E_{x3} \quad (47)$$

Where lateral electric field components in the region I, II, III are obtained using (42), (43), (44) and (45) given as

$$E_{x1} = -\frac{d\varphi_{s1}(x)}{dx} \left(1 + \frac{\varepsilon_1}{\varepsilon_2} \right) \quad (48)$$

$$E_{x2} = -\frac{d\varphi_{s2}(x)}{dx} \left(1 + \frac{\varepsilon_1}{\varepsilon_2} \right) \quad (49)$$

$$E_{x3} = -\frac{d\varphi_{s3}(x)}{dx} \left(1 + \frac{\varepsilon_1}{\varepsilon_2} \right) \quad (50)$$

The drain current density is given as follows

$$I_{DS}(x)/W = qn_s(x)v_e(x) \quad (51)$$

Where W is the gate width, $v_e(x)$ is the electron effective velocity, and is given as

$$v_e(x) = \frac{\mu_n E_x v_{sat}}{\mu_n E(x) + v_{sat}} \quad (52)$$

Where electron mobility μ_n is given as per the negative differential mobility model from [21]

$$\mu_n = \frac{\mu_{n0} + \frac{v_{sat}}{E_x} \left(\frac{E_x}{E_C}\right)^\gamma}{1 + \left(\frac{E_x}{E_C}\right)^\gamma} \quad (53)$$

For β -Ga₂O₃, the parameters $\mu_{n0} = 140 \text{ cm}^2/\text{Vs}$, $v_{sat} = 1.5 \times 10^7 \text{ cm/s}$, critical field $E_C = 2.25 \times 10^5 \text{ V/cm}$, and $\gamma = 2.84$ are taken from [24]. After substituting n_s from (17), the drain current given by (51) can be rewritten as

$$I_{DS}(x) = WC_G(V_{GO} - E_F) \frac{\mu_n E_x v_{sat}}{\mu_n E_x + v_{sat}} \quad (54)$$

4. Results and Discussion

The simulation results for the device structure (Fig. 1) are obtained using the 2D device simulator—ATLAS [21]. The physics-based models and material properties are discussed in previous sections. The device simulator is first calibrated with experimental results measured in [5]. The mathematical model data are obtained using the computational tool—MATLAB [25]. The surface potential profile, channel potential, and electric field profile are extracted from structure files saved at different bias voltages. The surface potential plots are shown in Fig. 2. These data are extracted from at the heterointerface of different structure files for three different V_{GS} of 1 V, -1 V, and -3 V and constant V_{DS} of 10 V. The computed data from derived model (41) are also shown.

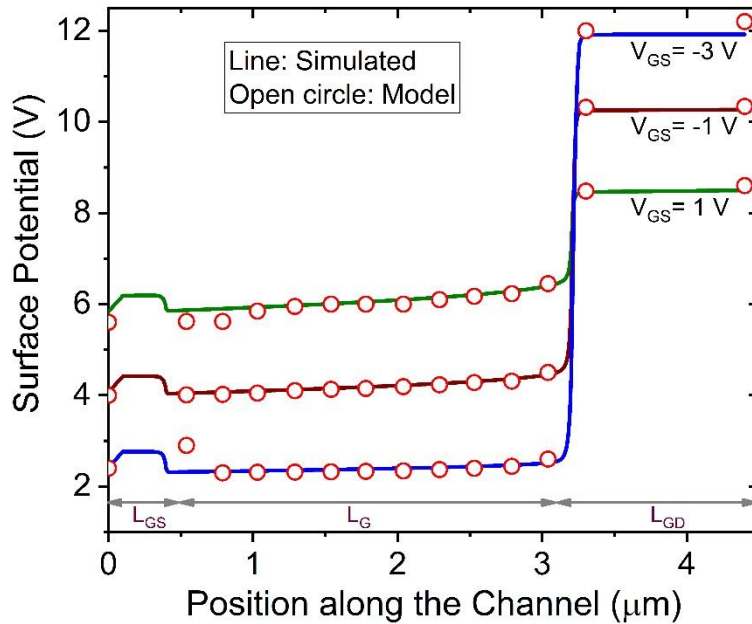


Fig. 2: The surface potential at the AlN/ β -Ga₂O₃ interface for different $V_{GS} = 1, -1, -3 \text{ V}$ at fixed $V_{DS} = 10 \text{ V}$. Full channel length subdivided into L_{GS} , L_G , and L_{GD} is also drawn in the lower part of the figure.

The channel potential and electric field simulated data are extracted in the channel 5 nm below the AlN/ β -Ga₂O₃ interface. The model data for channel potential and electric field are computed from (42), and (47) respectively. Simulated and model data for channel potential and electric field are shown in Fig. 3, and Fig. 4 respectively.

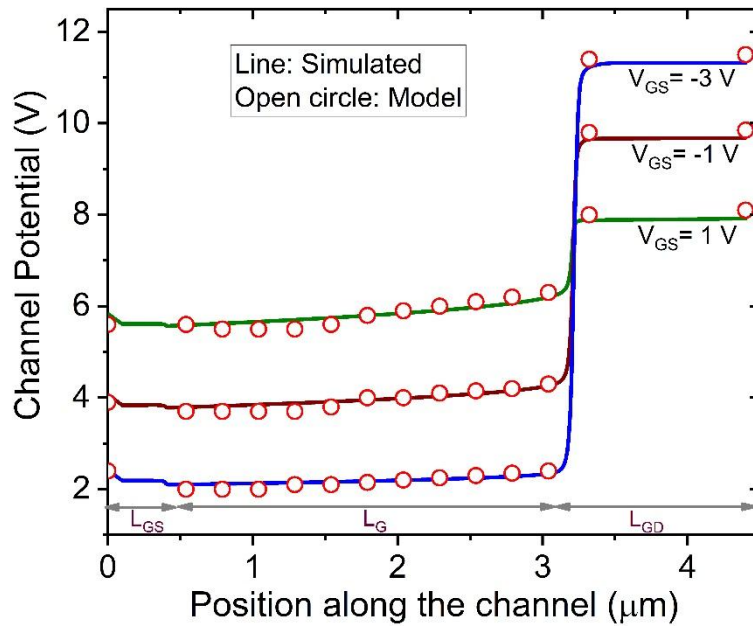


Fig. 3: Simulated and modeled data of channel potential along the channel below 5 nm from heterointerface for different $V_{GS} = 1, -1, -3$ V at fixed $V_{DS} = 10$ V. The plot is almost similar to surface potential plot except under L_{GS} in the latter.

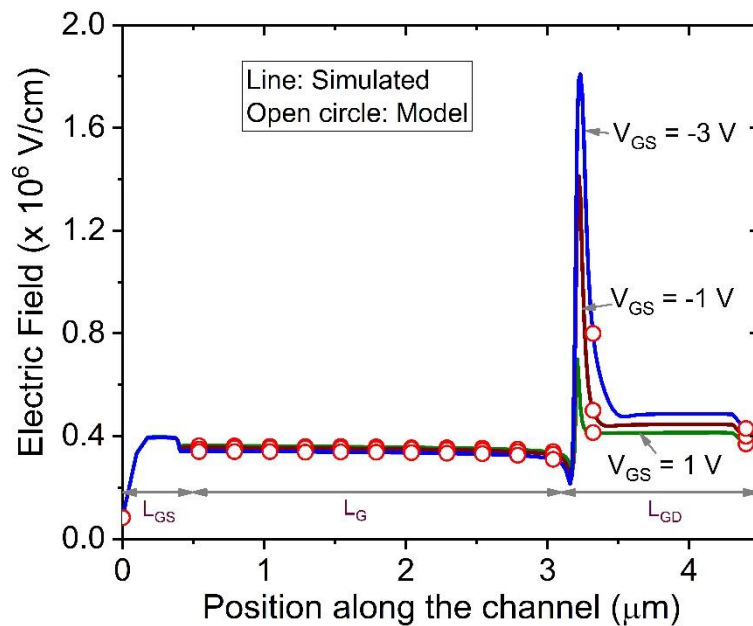


Fig. 4: Lateral electric field along the channel below 5 nm from heterointerface for different $V_{GS} = 1, -1, -3$ V at fixed $V_{DS} = 10$ V. Peak electric field of 1.8×10^6 V/cm is evident under the drain side gate edge.

The transfer characteristic of the proposed device is shown in Fig. 5. Drain current model data and experimental result relating to similar dimension device is also indicated. Except for the sub-threshold region, there is a good consistency between model data and simulation results. Additionally, a fair degree of agreement is evident with experimental data reported in [5].

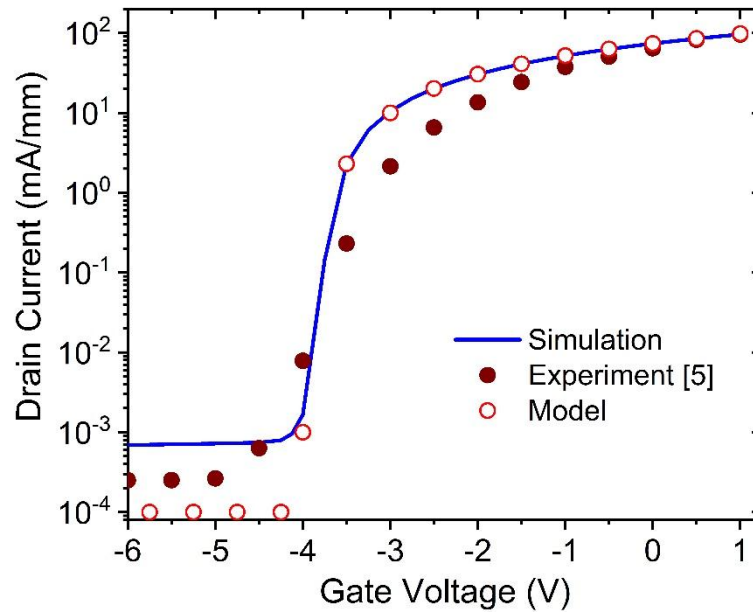


Fig. 5: Simulated, Experimental, and modeled data of $I_D - V_G$ characteristics of the analysed device.

5. Conclusion

The analytical model of surface potential, channel potential, and electric field for AlN/ β -Ga₂O₃ is presented. The 2D Poisson equation is solved to develop an expression of potential and lateral field along the channel and consequently extended to find expression of drain current. For the validation of the simulation and model data, the simulation deck is calibrated with device dimensions similar to the experimental one as reported elsewhere. Analytical model data of surface potential, channel potential, and electric field are rigorously validated with different values of gate voltages. Furthermore, drain current model results are compared with simulation results as well as validated by experimental data. A good level of agreement among all three is obtained. Further work in the physics-based analytical models for the β -Ga₂O₃-based devices can be helpful to understand device mechanism and useful to predict its potential for futuristic high power applications.

References:

- [1] Z. Hu *et al.*, "Field-Plated Lateral β -Ga₂O₃ Schottky Barrier Diode with High Reverse Blocking Voltage of More Than 3 kV and High DC Power Figure-of-Merit of 500 MW/cm²," *IEEE Electron Device Lett.*, pp. 1–1, 2018, doi: 10.1109/LED.2018.2868444.
- [2] J. Yang, F. Ren, M. Tadjer, S. J. Pearton, and A. Kuramata, "Ga₂O₃ Schottky rectifiers with 1 ampere forward current, 650 v reverse breakdown and 26.5 MW.cm⁻² figure-of-merit," *AIP Adv.*, vol. 8, no. 5, 2018, doi: 10.1063/1.5034444.
- [3] M. Higashiwaki *et al.*, "Depletion-mode Ga₂O₃ metal-oxide-semiconductor field-effect transistors on β -Ga₂O₃ (010) substrates and temperature dependence of their device characteristics," *Appl. Phys. Lett.*, vol. 103, no. 12, pp. 1–5, 2013, doi: 10.1063/1.4821858.
- [4] A. J. Green *et al.*, "3.8-MV/cm Breakdown Strength of MOVPE-Grown Sn-Doped β -Ga₂O₃ MOSFETs," *IEEE Electron Device Lett.*, vol. 37, no. 7, pp. 902–905, 2016, doi: 10.1109/LED.2016.2568139.
- [5] Z. Xia *et al.*, "Delta Doped β -Ga₂O₃ Field Effect Transistors With Regrown Ohmic Contacts," *IEEE Electron Device Lett.*, vol. 39, no. 4, pp. 568–571, Apr. 2018, doi: 10.1109/LED.2018.2805785.
- [6] Z. Feng *et al.*, "Normally-Off- β -Ga₂O₃ Power MOSFET with Ferroelectric Charge Storage Gate Stack Structure," *IEEE Electron Device Lett.*, vol. 41, no. 3, pp. 333–336, 2020, doi: 10.1109/LED.2020.2970066.
- [7] S. Krishnamoorthy *et al.*, "Modulation-doped β -(Al_{0.2}Ga_{0.8})₂O₃/Ga₂O₃ field-effect transistor," *Appl. Phys. Lett.*, vol. 111, no. 2, p. 023502, Jul. 2017, doi: 10.1063/1.4993569.
- [8] Y. Zhang *et al.*, "Demonstration of high mobility and quantum transport in modulation-doped β -(Al_xGa_{1-x})₂O₃/Ga₂O₃ heterostructures," *Appl. Phys. Lett.*, vol. 112, no. 17, pp. 1–6, 2018, doi: 10.1063/1.5025704.
- [9] W. Wei *et al.*, "Valence band offset of β -Ga₂O₃/wurtzite GaN heterostructure measured by X-ray photoelectron spectroscopy," *Nanoscale Res. Lett.*, vol. 7, no. 1, p. 562, 2012, doi: 10.1186/1556-276X-7-562.

- [10] H. Sun *et al.*, “Valence and conduction band offsets of β -Ga₂O₃/AlN heterojunction,” *Appl. Phys. Lett.*, vol. 111, no. 16, p. 162105, Oct. 2017, doi: 10.1063/1.5003930.
- [11] J.-X. Chen *et al.*, “Band alignment of AlN/ β -Ga₂O₃ heterojunction interface measured by x-ray photoelectron spectroscopy,” *Appl. Phys. Lett.*, vol. 112, no. 26, p. 261602, Jun. 2018, doi: 10.1063/1.5035372.
- [12] S. Lyu and A. Pasquarello, “Band alignment at β -Ga₂O₃/III-N (III = Al, Ga) interfaces through hybrid functional calculations,” *Appl. Phys. Lett.*, vol. 117, no. 10, p. 102103, Sep. 2020, doi: 10.1063/5.0020442.
- [13] R. Singh, T. R. Lenka, R. T. Velpula, B. Jain, H. Q. T. Bui, and H. P. T. Nguyen, “A novel β -Ga₂O₃ HEMT with fT of 166 GHz and X-band POUT of 2.91 W/mm,” *Int. J. Numer. Model. Electron. Networks, Devices Fields*, vol. 34, no. 1, pp. 1–11, 2021, doi: 10.1002/jnm.2794.
- [14] R. Singh, T. R. Lenka, and H. P. T. Nguyen, “Analytical Study of Conduction Band Discontinuity Supported 2DEG Density in AlN/ β -Ga₂O₃ HEMT,” *Facta Universitatis, Series: Electronics and Energetics*, 06 May 2021. (Accepted, in press)
- [15] S. P. Kumar, A. Agrawal, R. Chaujar, S. Kabra, M. Gupta, and R. S. Gupta, “Threshold voltage model for small geometry AlGa_N/Ga_N HEMTs based on analytical solution of 3-D Poisson’s equation,” *Microelectronics J.*, vol. 38, no. 10–11, pp. 1013–1020, 2007, doi: 10.1016/j.mejo.2007.09.001.
- [16] S. Khandelwal, N. Goyal, and T. A. Fjeldly, “A physics-based analytical model for 2DEG charge density in AlGa_N/Ga_N HEMT devices,” *IEEE Trans. Electron Devices*, vol. 58, no. 10, pp. 3622–3625, 2011, doi: 10.1109/TED.2011.2161314.
- [17] S. Khandelwal and T. A. Fjeldly, “A physics based compact model of I-V and C-V characteristics in AlGa_N/Ga_N HEMT devices,” *Solid. State. Electron.*, vol. 76, pp. 60–66, 2012, doi: 10.1016/j.sse.2012.05.054.
- [18] F. M. Yigletu, S. Khandelwal, T. A. Fjeldly, and B. Iniguez, “Compact charge-based physical models for current and capacitances in AlGa_N/Ga_N hemts,” *IEEE Trans. Electron Devices*, vol. 60, no. 11, pp. 3746–3752, 2013, doi: 10.1109/TED.2013.2283525.
- [19] M. Kaddeche, A. Telia, and A. Soltani, “Analytical modeling and analysis of Al_mGa_{1-m}N/Ga_N HEMTs employing both field-plate and high-k dielectric stack for high-voltage operation,” *J. Comput. Electron.*, vol. 12, no. 3, pp. 501–510, 2013, doi: 10.1007/s10825-013-0468-5.
- [20] S. Khandelwal, S. Ghosh, Y. S. Chauhan, B. Iniguez, and T. A. Fjeldly, “Surface-Potential-Based RF Large Signal Model for Gallium Nitride HEMTs,” *2015 IEEE Compd. Semicond. Integr. Circuit Symp. CSICS 2015*, pp. 1–4, 2015, doi: 10.1109/CSICS.2015.7314527.
- [21] Device Simulation Software, ATLAS User’s Manual, Silvaco, Santa Clara, CA, USA, 2019.
- [22] A. Mock *et al.*, “Band-to-band transitions, selection rules, effective mass, and excitonic contributions in monoclinic β -Ga₂O₃,” *Phys. Rev. B*, vol. 96, no. 24, pp. 1–14, 2017, doi: 10.1103/PhysRevB.96.245205.
- [23] S. Ponc e and F. Giustino, “Structural, electronic, elastic, power, and transport properties of β -Ga₂O₃ from first principles,” *Physical Review Research*, vol. 2, no. 3, p. 033102, 2020, [Online]. Available: <https://link.aps.org/doi/10.1103/PhysRevResearch.2.033102>.
- [24] K. Ghosh and U. Singisetti, “Ab initio velocity-field curves in monoclinic β -Ga₂O₃,” *J. Appl. Phys.*, vol. 122, no. 3, p. 035702, Jul. 2017, doi: 10.1063/1.4986174.
- [25] MATLAB Version 7.10.0 (R2018a). Natick, Massachusetts: The MathWorks Inc.; 2018.